Title	Elementary electron and ion dynamics in ionized liquid water
Author(s)	Li, Jialin.; Nie, Zhaogang.; Zheng, Yi Ying.; Dong, Shuo.; Loh, Zhi-Heng.
Citation	Li, J., Nie, Z., Zheng, Y. Y., Dong, S., & Loh, Z. H. (2013). Elementary electron and ion dynamics in ionized liquid water. The Journal of Physical Chemistry Letters, 4, 3698 -3703.
Date	2013
URL	http://hdl.handle.net/10220/17346
Rights	© 2013 American Chemical Society. This is the author created version of a work that has been peer reviewed and accepted for publication by The Journal of Physical Chemistry Letters, American Chemical Society. It incorporates referee's comments but changes resulting from the publishing process, such as copyediting, structural formatting, may not be reflected in this document. The published version is available at: [http://dx.doi.org/10.1021/jz401987f].

Elementary Electron and Ion Dynamics in Ionized Liquid Water

Jialin Li,[†] Zhaogang Nie,[†] Yi Ying Zheng,[†] Shuo Dong,[†] Zhi-Heng Loh[*,†]

[†] Division of Chemistry and Biological Chemistry, and Division of Physics and Applied Physics, School of Physical and Mathematical Sciences, Nanyang Technological University, Singapore 637371, Singapore

[*] Electronic mail: zhiheng@ntu.edu.sg

Abstract

The ionization of liquid water functions as the principal trigger for a myriad of phenomena that are relevant to radiation chemistry and biology. The earliest events that follow the ionization of water, however, remain relatively unknown. Here, femtosecond coherence spectroscopy is combined with polarization anisotropy measurements to elucidate the ultrafast electron and ion dynamics in ionized water. The results show that strong-field ionization of liquid water produces an aligned *p* electron distribution. Furthermore oscillations observed in the polarization anisotropy are suggestive of valence electron motion in the highly reactive H_2O^+ radical cation, whose lifetime with respect to proton transfer is found to be 196 ± 5 fs. Coherent intermolecular motions that signal initial solvent reorganization and subsequent long-lived ballistic proton transport that involves the H_3O^+ end-product are also detected in the time domain. These results offer new insight into the elementary dynamics of ionized liquid water.

TOC Graphic

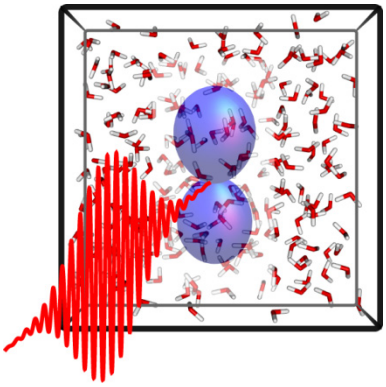

Keywords: Ultrafast spectroscopy, hydrated electron, valence electron motion, hydrogen bond, proton transfer, photoelectron angular distribution

The ionization of liquid water is a universal phenomenon that accompanies the interaction of high-energy radiation with matter in aqueous environments. The ensuing cascade of chemical reactions that involves ions, electrons, and radicals forms the basis of solution and interfacial radiation chemistry.[1] Moreover, since liquid water comprises the major component of cellular matter, oxidative damage to biological systems by high-energy radiation is triggered mainly by the ionization of water.[2] The low-energy electrons that are produced by ionization can also induce radiation damage by dissociative electron attachment to biomolecules.[3] The elementary processes that follow the ionization of liquid water therefore forms the fundamental framework for studies of radiation-matter interaction in chemistry and biology.

The direct products of water ionization are the H_2O^+ radical cation and the hydrated electron,[1] both of which are highly reactive species. Ab initio molecular dynamics (AIMD) simulations[4,5] and infrared spectroscopy of ionized water clusters[6] show that H_2O^+ undergoes an ion-molecule reaction with a neighboring H_2O molecule to yield the hydronium cation (H_3O^+) and a hydroxyl radical (OH). The H_3O^+ product subsequently undergoes rapid structural diffusion, akin to the case of an excess proton in water,[7] thereby resulting in the rapid disappearance of the initial $H_3O^+\cdots OH$ contact pair. The predicted time scale for the proton transfer from H_2O^+ is ~100 fs,[4,5] although experimental attempts at the determination of its lifetime have thus far been inconclusive.[5,8,9]

In contrast to the elusive H_2O^+ cation, the spectroscopy and dynamics of the hydrated electron has been studied extensively.[10] The transition of the hydrated electron from the *s*-like ground state to the *p*-like excited state underlies its absorption spectrum, which peaks at 719 nm and spans <500 – 1000 nm.[11] Time-resolved optical pump-probe spectroscopy elucidates the ultrafast dynamics following either the injection of an electron into water by multiphoton

ionization (MPI)[9,12] or the photoexcitation of a pre-equilibrated hydrated electron.[13,14] The latter studies reveal subpicosecond dynamics with time constants of ~50 fs and ~300 fs, whereby the faster component exhibits a pronounced H/D isotope dependence. The short-time dynamics is ascribed to inertial solvation of the *p* state (adiabatic solvation model)[13] or alternatively, to internal conversion of the *p* state to a vibrationally hot *s* state (nonadiabatic solvation model);[14] recent femtosecond photoelectron imaging experiments performed on anionic water clusters lend support to the nonadiabatic solvation model.[15] Similarly, studies of the hydrated electron generated by MPI reveal the solvation dynamics of the *s* state electron, although the intermediary *p* state electron has eluded direct spectroscopic observation.[16–19]

Here, femtosecond coherence spectroscopy[20–22] is combined with polarization anisotropy measurements to investigate the early-time electron and ion dynamics triggered by the MPI of liquid water. The peak intensity of the 800-nm ionization pump pulse (2×10^{13} W/cm^2) yields a Keldysh parameter of $\gamma \sim 2$ (see Supporting Information). Accordingly the MPI process can be characterized as being in the strong-field regime. Fluence dependence measurements reveal a 9-photon MPI process (see Supporting Information); ionization channels that involve 5- and 6-photon resonance enhancement are accessible at this laser wavelength.[23] The total energy deposition of 14.0 eV is significantly above the vertical ionization potential of liquid water (11.16 eV).[24] At this input energy, the large electron ejection length of $\langle r_0 \rangle \sim 35$ Å,[25] which defines the spatial extent of the surrounding medium over which the electron is delocalized, allows access to the collective dynamics of up to ~10^4 water molecules. The 800-nm probe pulse interrogates the $s \rightarrow p$ transitions of both the hydrated *s* electron and its pre-solvated precursor.[26,18] The manner in which the intermolecular vibrational coherences of liquid water modulates the electron $s \rightarrow p$ absorption is analogous to the way in which a vibrational wave packet that is

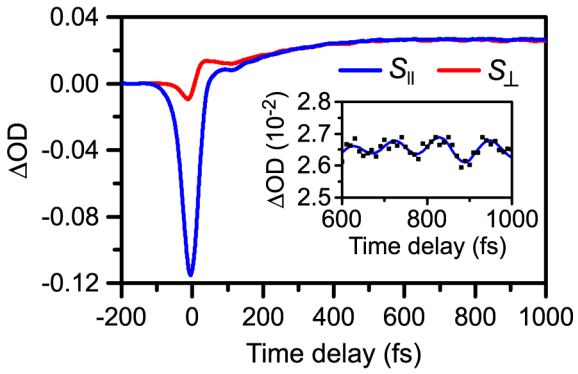

Figure 1. Femtosecond time-resolved differential absorption signal (ΔOD) as a function of time delay for parallel ($S_{\parallel}$) and perpendicular ($S_{\perp}$) relative polarizations between pump and probe beams. The inset shows the $S_{\parallel}$ signal at later time delays, during which an oscillation is apparent.

launched on a molecular potential energy surface modifies the energy and amplitude of its associated electronic transitions.[27,28] By relying on the observation of coherences and polarization anisotropies that are associated with the various intermediates, our approach complements earlier methods based on optical pump-probe transient absorption (TA) spectroscopy, which has its limitations. For example, the inability to isolate the H_2O^+ species in a recent femtosecond deep UV pump-supercontinuum probe TA experiment was attributed to its weak absorption being overwhelmed by the strong absorbance of the solvated electron.[5]

The time-dependent differential absorption time traces for parallel ($S_{\parallel}$) and perpendicular ($S_{\perp}$) relative pump-probe polarizations are shown in Figure 1. Beyond the region of pump-probe temporal overlap (–50 to +50 fs), where nonlinear effects that involve both pump and probe beams dominate, both $S_{\parallel}$ and $S_{\perp}$ are positive and show an overall increase with time delay that can be attributed to the formation of the hydrated *s* electron. The ionization fraction is estimated to be 7×10^{-6} based on the differential absorbance measured at 1-ps time delay and the known molar extinction coefficient of the hydrated electron at 800 nm (1.6×10^4 $M^{-1}cm^{-1}$).[26] Note that the recombination of the hydrated electron with OH and/or H_3O^+ do not contribute significantly

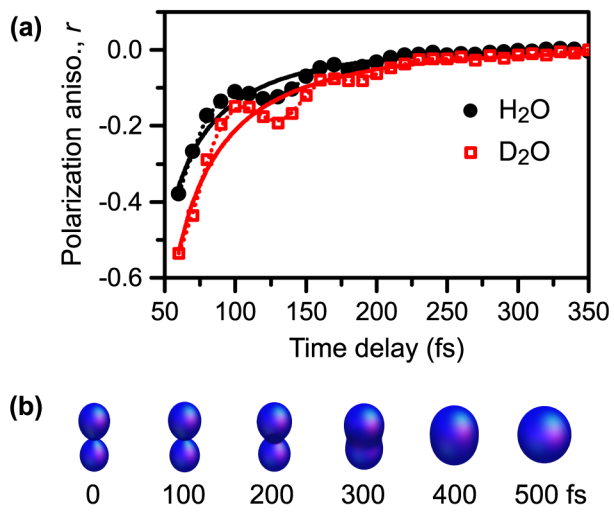

Figure 2. (a) The polarization anisotropy *r* shows that the *p* electron is produced by the MPI of liquid water. The symbols correspond to the experimental data. The solid lines are obtained from the fits to the theoretical model (see main text). (b) Time-evolution of the *p* state electron angular distribution in liquid H_2O, as reconstructed from experimental data.

to the dynamics that occur within the 1-ps time delay investigated here.[29,30] Furthermore, the >90% transmission of the ionizing pump beam through the sample (before accounting for reflection losses) implies minimal heating of the water target (<1 K temperature rise) by the pump beam, either by OH overtone absorption[31] or by multiphoton excitation.[32] Finally, the use of a strong-field pump pulse confines ionization to sub-optical-cycle durations,[33] thereby suppressing photodissociation that involve neutral electronically excited states,[34,35] some of which in the gas phase can occur on the few-femtosecond time scale.[36]

The polarization anisotropy observed at early times provides direct evidence for the creation of an aligned electron by the MPI of liquid water (Figure 2a). The time-dependent polarization anisotropy is modeled by considering that strong-field ionization by a laser pulse with electric field polarized along the *z* direction produces an incoherent mixture of *s* and p_z electrons with initial fractional populations $f_s(0)$ and $f_p(0)$, respectively (see Supporting Information). The model further assumes that the p_z excited state relaxes to the *s* ground state

with a decay lifetime τ_p. While electron states with higher angular momenta can be populated by ionization, the angular momenta states that are included in our model are restricted to the *s* and *p* states, due to the predominant sensitivity of the 800-nm probe wavelength to the $s \rightarrow p$ transition, as well as the limitations on the number of independent variables that can be extracted from the data. Moreover omission of the p_x and p_y electrons from the above consideration is motivated by previous work on gas-phase atomic and molecular strong-field MPI, which show that angular distributions of the ejected electrons are primarily aligned along the polarization axis of the ionization pump pulse.[37,38] Fitting of the polarization anisotropy with only $f_p(0)$ and τ_p as adjustable parameters yields, in the case of H_2O (D_2O), values of 0.94 ± 0.05 (0.92 ± 0.04) for $f_p(0)$ and 79 ± 5 fs (101 ± 6 fs) for τ_p (Figure 2a). The reconstructed temporal evolution of the electron angular distribution following the ionization of liquid H_2O is shown in Figure 2b.

The creation of an aligned electron distribution in this work is facilitated by the use of a strong-field-ionizing pump pulse, whereas it should be noted that previous MPI studies of liquid water were performed with pump pulse intensities that are in the perturbative regime. While the initial fractional populations of the p_z electron generated in H_2O and D_2O are identical to within experimental error, the retrieved *p* state lifetimes are clearly dependent on H/D isotopic substitution, with the lifetime being longer in D_2O than in H_2O by a factor of 1.3 ± 0.1; note that a more negative anisotropy at 60-fs time delay in D_2O than in H_2O is consistent with the longer *p* electron lifetime in the former (Figure 2a). This result is reminiscent of that obtained from previous studies of the *p* electron dynamics that follows the photoexcitation of the pre-equilibrated *s* electron.[14,15] In those studies, the factor-of-$\sqrt{2}$ slowdown observed in the internal conversion dynamics upon deuteration is attributed to the participation of librational modes in electronic relaxation. In fact, we note the similarity in relaxation time scales for the *p* electron

prepared by MPI and that obtained within the nonadiabatic solvation model of photoexcited hydrated electron dynamics.[14,15] The H/D substitution dependence observed here therefore suggests that solvent librational modes mediate the relaxation of the injected *p* state electron prior to its solvation. The slightly longer lifetime of *p* electrons produced by MPI than by photoexcitation can be rationalized in terms of differing initial conditions: the solvation of an electron following the ionization of water is likely to involve a larger solvent reorganization penalty than the solvation of a partially hydrated *p* electron produced by photoexcitation.

Oscillatory features in the polarization anisotropy decay indicate a periodic reorientation of the probe transition dipole moment that is concomitant with the electronic relaxation of the *p* state electron. The residual polarization anisotropies, obtained by subtracting the fits for the *p* electron population decay from the polarization anisotropy signals over a time delay range of 60 – 350 fs, are shown in Figure 3a for both H_2O and D_2O. Their corresponding Fast Fourier Transform (FFT) power spectra reveal oscillation frequencies of 150 cm^{-1} and 500 cm^{-1} (Figure 3b, solid lines), neither of which exhibits a perceptible shift with H/D substitution. Time-domain analysis yields, for the case of H_2O (D_2O), cosinusoidal phases (in units of π rad) of -0.31 ± 0.09 (-0.39 ± 0.09) and 1.30 ± 0.08 (1.00 ± 0.04) for the low- and high-frequency component, respectively (see Supporting Information). The exponential damping times of both frequency components in the oscillations are 70 ± 12 fs and 64 ± 7 fs for H_2O and D_2O, respectively. For comparison, the FFT power spectra of the isotropic signals S_{iso}, where $S_{iso} = (S_{\parallel} + 2S_{\perp})/3$ (Figure 3b, dashed lines), exhibit only one frequency component at 150 cm^{-1}.

A possible source of the 500-cm^{-1} polarization anisotropy modulation is solvent librational motion. The sub-100-fs lifetime of librational excitation, as elucidated by ultrafast infrared spectroscopy[39] and molecular dynamics simulations,[40] is consistent with the ~70-fs

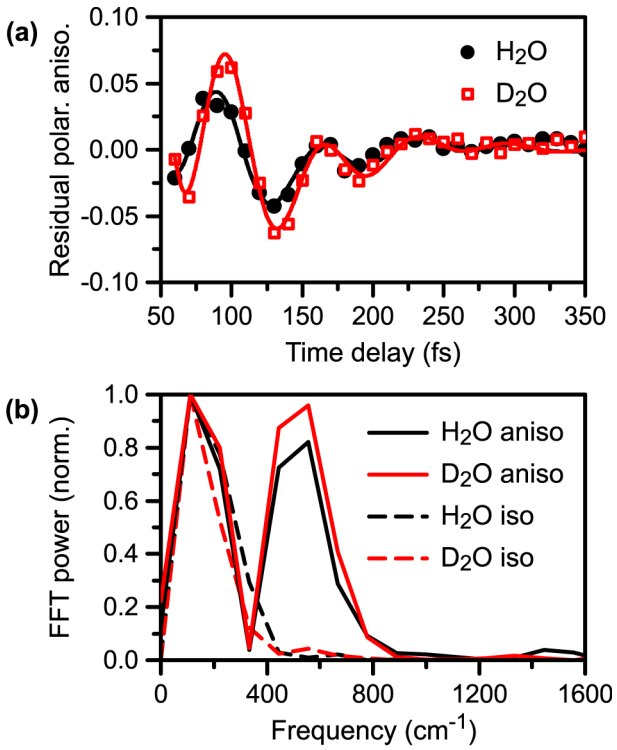

Figure 3. (a) The residual polarization anisotropy (symbols) reveals oscillatory features, which can be fit to a sum of two exponentially decaying cosinusoidal functions (solid lines). (b) The FFT power spectra of the residual polarization anisotropies reveal frequency components at 150 and 500 cm^{-1} (solid lines), both of which are independent of H/D substitution. For comparison, the FFT power spectra of the isotropic signals are also shown (dashed lines).

decay of the polarization anisotropy oscillation observed here. Despite the broad FFT frequency linewidth, however, it is unclear as to why the 500-cm^{-1} component is centered on the L_1 librational band of H_2O, even though the L_2 band at 780 cm^{-1}, which extends to ~1000 cm^{-1}, bears considerable Raman intensity.[41] Furthermore the 500-cm^{-1} band does not shift with H/D isotope substitution, even though the librational frequencies of D_2O are lower than those of H_2O by ~$\sqrt{2}\times$.

In addition to librational motion, another potential explanation for the 500-cm^{-1} component is angular reorientation via electron motion. Indeed, previous studies of multichromophoric systems have shown that coherent electronic energy transfer leads to

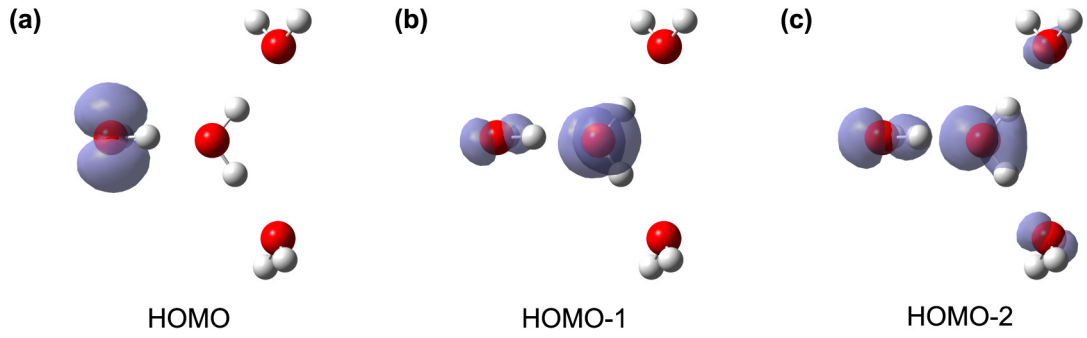

Figure 4. Orbital densities of the (a) HOMO, (b) HOMO–1, and (c) HOMO–2 of $(H_2O)_4$. Note the orthogonal directions of the dominant orbital densities of the different molecular orbitals, which suggests that their coherent superposition would give rise to a periodic reorientation of the hole density in the $(H_2O)_4^+$ ion.

oscillations in the polarization anisotropy signal that are absent in the isotropic signal.[42] It has recently been shown that the strong-field MPI of atoms can trigger valence electron motion in the resultant ions, for which the ~1-eV energy spacing ΔE between valence electronic states leads to few-femtosecond oscillation periods $T_{el} = h/\Delta E$.[43,44] In the case of liquid water, the initiation of valence electron motion by strong-field MPI is favored by its dense manifold of electronic states, which presents aqueous H_2O^+ ion states with energetic separations that are commensurate with the 500-cm^{-1} oscillation frequency observed here.[45,46] Furthermore a recent theoretical study suggests that the sudden ionization of the water dimer induces the oscillation of charge density between the oxygen centers of the $(H_2O)_2^+$ cation.[47] Our ab initio calculations on the $(H_2O)_4$ model cluster suggests, within a Koopman-type picture, the common occurrence of $(H_2O)_4^+$ ion states with orthogonal hole densities. For example, the orbital densities of the HOMO, HOMO–1, and HOMO–2 orbitals of $(H_2O)_4$, which correspond to the hole densities of the three lowest $(H_2O)_4^+$ ion states, are each oriented in perpendicular directions (Figure 4). The coherent superpositions of these ion states leads to a periodic reorientation of the hole density, which in turn modulates the alignment of the *p* electron via the Coulomb interaction, from which

an oscillatory component in the polarization anisotropy results. The coherent electronic origin of the observed 500-cm^{-1} oscillation is further supported by its cosinusoidal phase of ~π rad, which implies a polarization anisotropy that begins at its negative extremum. That is, the hole density at the moment of ionization is maximally aligned, as observed previously for coherent atomic ion states prepared by strong-field MPI.[44] It is important to note here that the ~70-fs dephasing time of the hole coherence is not limited by the 1.6-fs optical dephasing time of the $s \rightarrow p$ transition of the hydrated electron.[48,49]

The 150-cm^{-1} component that arises in both isotropic and polarization anisotropy signals is assigned to a Raman-active intermolecular hindered translation along the hydrogen bond coordinate.[41] From previous time-domain optical Kerr effect studies of pure water[50] and aqueous salt solutions,[51] the emergence of this mode in S_{iso}, despite its near-complete Raman depolarization for pure liquid water,[41] is a manifestation of the solvent reorganization that follows the MPI of water. This conclusion is further supported by resonance Raman measurements[52] and theoretical calculations[53,54] on the hydrated *s* electron, which show that its photoexcitation is coupled to the hindered translation of solvent molecules. On the other hand, the appearance of the 150-cm^{-1} component in the polarization anisotropy is ascribed to hindered intermolecular translation that is driven by the periodic reorientation of the hole density. In support of this assignment, an ab initio calculation of the $(H_2O)_4^+$ radical cation reveals hindered translational modes with frequencies in the range of 140 – 210 cm^{-1} and depolarization ratios of 0.4 – 0.6 (see Supporting Information). The observed phase shift between the 500-cm^{-1} and 150-cm^{-1} frequency components can be rationalized in terms of the nonadiabatic driving of the hindered translational mode by the electron motion.

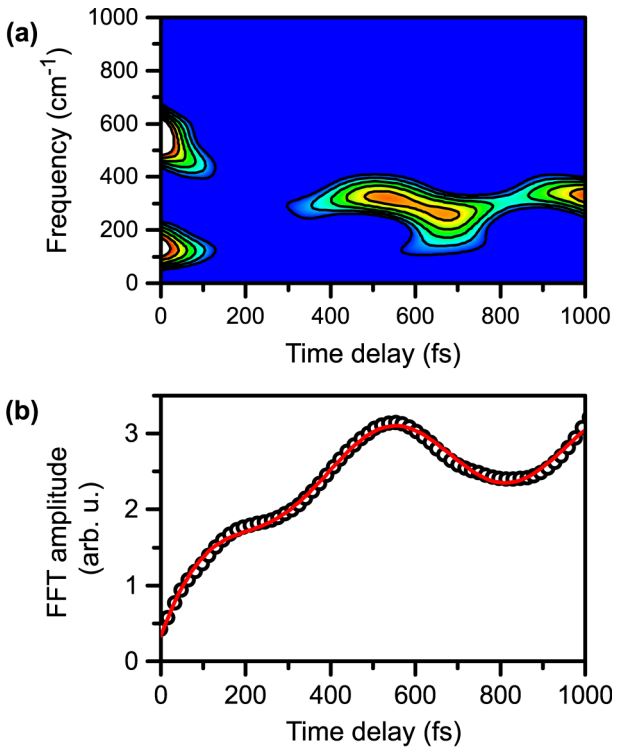

Figure 5. (a) The time-frequency spectrogram for the anisotropic signal shows the disappearance of the 150 and 500 cm^{-1} frequency components at early times and the concomitant rise of the frequency component at 310 cm^{-1}. (b) The FFT amplitude at 310 cm^{-1} reveals an oscillatory rise (symbol), from which a fit to first-order kinetics (solid line) yields a lifetime of 196 ± 5 fs for the aqueous H_2O^+ radical cation.

The time-frequency spectrogram derived from the anisotropic signal $S_{aniso} = S_{\parallel} - S_{\perp}$ (Figure 5) shows the decay of frequency components at 150 cm^{-1} and 500 cm^{-1} and the appearance of a 310-cm^{-1} component. The new frequency component originates from the oscillatory feature that extends to 1 ps in both $S_{\parallel}$ and $S_{\perp}$ signals (Figure 1 inset). Note that the center frequency of the nominal 310-cm^{-1} component shifts periodically in the range of 260 – 330 cm^{-1}; the period of the shift corresponds to a frequency of 60 cm^{-1}.

The feature at 310 cm^{-1}, which is independent of H/D substitution, is attributed to the hindered translation between water molecules and the H_3O^+ hydronium cation to which they are bound, *cf.* 175 cm^{-1} for pure water.[41] The vibrational frequency blueshift upon water protonation,

which implies the strengthening of the hydrogen bond, is consistent with the contraction of the intermolecular O···O distance from 2.85 Å in pure water to 2.52 Å in aqueous acid.[55] This assignment is further supported by ab initio results for the Zundel ion ($H_9O_4^+$), which reveal hindered translational modes involving the central H_3O^+ moiety and the peripheral H_2O molecules at 270 cm^{-1} and 330 cm^{-1} (see Supporting Information). The latter, being the asymmetric combination, is completely depolarized and is therefore expected to feature prominently in the anisotropic signal. The 60-cm^{-1} modulation of the hindered translation mode suggests that this mode is coupled to the hydrogen bond bending vibration.[41]

The extended appearance of the 310-cm^{-1} frequency component in the spectrogram signifies long-lived coherent intermolecular hindered translational motion that accompanies ballistic proton transport. This vibrational coherence is reaction-driven,[56,57] in this case, by the strongly exergonic initial proton transfer from H_2O^+ to a neighboring water molecule. AIMD studies show that this intermolecular vibrational mode drives excess proton transport in water: the proton donor and proton acceptor water molecules must first approach one another before proton transfer is energetically feasible.[7,58] Moreover, the observed ballistic proton transport agrees with the non-diffusive nature of proton transfer predicted by AIMD simulations of ionized liquid water.[59]

Since H_3O^+ is initially produced by the transfer of a proton from the H_2O^+ radical cation to a neighboring water molecule, the onset of ballistic proton transport is expected to correlate with the population decay of the H_2O^+ species. Fitting the growth of the 310-cm^{-1} frequency component to pseudo-first-order kinetics yields a lifetime of 196 ± 5 fs for the H_2O^+ radical cation. This experimentally determined lifetime is significantly longer than the ~100-fs lifetime predicted by AIMD simulations.[5] However we note that the simulations did not consider the

presence of a hydrated electron, or the possibility that aqueous H_2O^+ could exist as a coherent superposition of delocalized ion states. It is possible that solvent reorganization to accommodate the injected electron competes with the solvation of H_2O^+, thereby impeding proton transfer to produce H_3O^+. Moreover, the $H_2O^+\cdots H_2O$ bond contraction that is necessary for proton transfer[5] from H_2O^+ occurs on a time scale that is ~3× slower than the coherent charge oscillation of the aqueous H_2O^+ hole density. The altering identity of the proton donor conceivably frustrates the proton transfer step, thus prolonging the lifetime of the H_2O^+ radical cation.

The present work offers a glimpse of the multitude of hitherto unobserved elementary electron and ion dynamics that are triggered by the ionization of liquid water. These experimental results provide strong impetus for the development of a comprehensive theoretical treatment of liquid water ionization that considers the coupled dynamics of the injected electron, the H_2O^+ radical cation, and the solvent medium. Furthermore, it is envisioned that experiments with improved time resolution will uncover coherent dynamics that evolve on shorter time scales, such as those triggered by core-level ionization,[60] or those related to intramolecular vibrational motion and/or electron motion involving different electronic bands. Finally, we emphasize that the coherent dynamics elucidated in this work remain pertinent to the study of water ionization by high-energy charged particles, since the rapid traversal of a charged particle through a molecule is equivalent to exposing the molecule to an ultrashort electromagnetic pulse.[61] With typical traversal times that easily approach the sub-femtosecond regime,[62] such high-energy charged particles could certainly trigger a vast array of coherent dynamics beyond those reported here.

Acknowledgments

We are greatly indebted to Prof. M. Parrinello and Dr. A. Hassanali for illuminating discussions. We also thank Prof. H.-S. Tan for an equipment loan, and Prof. C. Andreani, Prof. R. Santra and Dr. O. Vendrell for useful discussions. This work is supported by a start-up grant from NTU, the A*Star Science and Engineering Research Council Public Sector Funding (122-PSF-0011), and the award of a Nanyang Assistant Professorship to Z.-H.L.

Supporting Information

Experimental and computational methods, Cartesian coordinates of the optimized geometries of $(H_2O)_4$ and $H_9O_4^+$ obtained from ab initio calculations, calculated vibrational frequencies, Raman activities, and depolarization ratios of $(H_2O)_4^+$ and $H_9O_4^+$, results of fluence dependence measurements for the determination of the pump photon order, derivation of the theoretical model for fitting the polarization anisotropy decay, time-domain analysis of the residual polarization anisotropy decay, and calculation of the frequency-time spectrogram and its application to obtaining the lifetime of aqueous H_2O^+. This material is available free of charge via the Internet at http://pubs.acs.org.

REFERENCES

1. Garrett, B. C.; Dixon, D. A.; Camaioni, D. M.; Chipman, D. M.; Johnson, M. A.; Jonah, C. D.; Kimmel, G. A.; Miller, J. H.; Rescigno, T. N.; Rossky, P. J.; et al. Role of Water in Electron-Initiated Processes and Radical Chemistry: Issues and Scientific Advances. *Chem. Rev*. **2005**, *105*, 355–389.
2. Ward, J. F. DNA Damaged Produced by Ionizing Radiation in Mammalian Cells: Identities, Mechanisms of Formation, and Reparability. *Prog. Nucleic Acid Res. Mol. Biol*. **1988**, *35*, 95–125.
3. Huels, M. A.; Boudaïffa, B.; Cloutier, P.; Hunting, D.; Sanche, L. Single, Double, and Multiple Double Strand Breaks Induced in DNA by 3–100 eV Electrons. *J. Am. Chem. Soc*. **2003**, *125*, 4467–4477.
4. Furuhama, A.; Dupuis, M.; Hirao, K. Reactions Associated with Ionization in Water: A Direct Ab Initio Dynamics Study of Ionization in $(H_2O)_{17}$. *J. Chem. Phys*. **2006**, *124*, 164310.
5. Marsalek, O.; Elles, C. G.; Pieniazek, P. A.; Pluhařová, E.; VandeVondele, J.; Bradforth, S. E.; Jungwirth, P. Chasing Charge Localization and Chemical Reactivity Following Photoionization of Liquid Water. *J. Chem. Phys*. **2011**, *135*, 224510.
6. Mizuse, K.; Kuo, J.-L.; Fujii, A. Structural Trends of Ionized Water Networks: Infrared Spectroscopy of Water Cluster Radical Cations $(H_2O)_n^+$ (n = 3–11). *Chem. Sci*. **2011**, *2*, 868–876.
7. Marx, D.; Tuckerman, M. E.; Hutter, J.; Parrinello, M. The Nature of the Hydrated Excess Proton in Water. *Nature* **1999**, *397*, 601–604.

8. Gauduel, Y.; Pommeret, S.; Migus, A.; Antonetti, A. Some Evidence of Ultrafast H_2O^+–Water Molecule Reaction in Femtosecond Photoionization of Pure Liquid Water: Influence on Geminate Pair Recombination Dynamics. *Chem. Phys*. **1990**, *149*, 1–10.

9. Long, F. H.; Lu, H.; Eisenthal, K. B. Femtosecond Studies of the Presolvated Electron: An Excited State of the Solvated Electron? *Phys. Rev. Lett*. **1990**, *64*, 1469–1472.

10. Turi, L.; Rossky, P. J. Theoretical Studies of Spectroscopy and Dynamics of Hydrated Electrons. *Chem. Rev*. **2012**, *112*, 5641–5674.

11. Hart, E. J.; Boag, J. W. Absorption Spectrum of the Hydrated Electron in Water and in Aqueous Solutions. *J. Am. Chem. Soc*. **1962**, *84*, 4090–4095.

12. Migus, A.; Gauduel, Y.; Martin, J. L.; Antonetti, A. Excess Electrons in Liquid Water: First Evidence of a Prehydrated State with Femtosecond Lifetime. *Phys. Rev. Lett*. **1987**, *58*, 1559–1562.

13. Silva, C.; Walhout, P. K.; Yokoyama, K.; Barbara, P. F. Femtosecond Solvation Dynamics of the Hydrated Electron. *Phys. Rev. Lett*. **1998**, *80*, 1086–1089.

14. Pshenichnikov, M. S.; Baltuška, A.; Wiersma, D. A. Hydrated-Electron Population Dynamics. *Chem. Phys. Lett*. **2004**, *389*, 171–175.

15. Bragg, A. E.; Verlet, J. R. R.; Kammrath, A.; Cheshnovsky, O.; Neumark, D. M. Hydrated Electron Dynamics: From Clusters to Bulk. *Science* **2004**, *306*, 669–674.

16. Hertwig, A.; Hippler, H.; Unterreiner, A. N.; Vohringer, P. Ultrafast Relaxation Dynamics of Solvated Electrons in Water. *Ber. Bunsenges. Phys. Chem*. **1998**, *102*, 805–810.

17. Assel, M.; Laenen, R.; Laubereau, A. Femtosecond Solvation Dynamics of Solvated Electrons in Neat Water. *Chem. Phys. Lett*. **2000**, *317*, 13–22.

18. Vilchiz, V. H.; Kloepfer, J. A.; Germaine, A. C.; Lenchenkov, V. A.; Bradforth, S. E. Map for the Relaxation Dynamics of Hot Photoelectrons Injected into Liquid Water via Anion Threshold Photodetachment and Above Threshold Solvent Ionization. *J. Phys. Chem. A* **2001**, *105*, 1711–1723.

19. Kambhampati, P.; Son, D. H.; Kee, T. W.; Barbara, P. F. Solvated Dynamics of the Hydrated Electron Depends on its Initial Degree of Electron Delocalization. *J. Phys. Chem. A* **2002**, *106*, 2374–2378.

20. Rosker, M. J.; Wise, F. W.; Tang, C. L. Femtosecond Relaxation Dynamics of Large Molecules. *Phys. Rev. Lett*. **1986**, *57*, 321–324.

21. Gruebele, M.; Zewail, A. H. Femtosecond Wave Packet Spectroscopy: Coherences, the Potential, and Structural Determination. *J. Chem. Phys*. **1993**, *98*, 883–902.

22. Dhar, L.; Rogers, J. A.; Nelson, K. A. Time-Resolved Vibrational Spectroscopy in the Impulsive Limit. *Chem. Rev*. **1994**, *94*, 157–193.

23. Kerr, G. D.; Hamm, R. N.; Williams, M. W.; Birkhoff, R. D.; Painter, L. R. Optical and Dielectric Properties of Water in the Vacuum Ultraviolet. *Phys. Rev. A* **1972**, *5*, 2523–2527.

24. Winter, B.; Weber, R.; Widdra, W.; Dittmar, M.; Faubel, M.; Hertel, I. V. Full Valence Band Photoemission from Liquid Water Using EUV Synchrotron Radiation. *J. Phys. Chem. A* **2004**, *108*, 2625–2632.

25. Crowell, R. A.; Bartels, D. M. Multiphoton Ionization of Liquid Water with 3.0–5.0 eV Photons. *J. Phys. Chem*. **1996**, *100*, 17940–17949.

26. Jou, F.-Y.; Freeman, G. R. Temperature and Isotope Effects on the Shape of the Optical Absorption Spectrum of Solvated Electrons in Water. *J. Phys. Chem*. **1979**, *83*, 2383–2387.

27. Fragnito, H. L.; Bigot, J.-Y.; Becker, P. C.; Shank, C. V. Evolution of the Vibronic Absorption Spectrum in a Molecule Following Impulsive Excitation with a 6 fs Optical Pulse. *Chem. Phys. Lett*. **1989**, *160*, 101–104.

28. Pollard, W. T.; Mathies, R. A. Analysis of Femtosecond Dynamics Absorption Spectra of Nonstationary States. *Annu. Rev. Phys. Chem*. **1992**, *43*, 497–523.

29. Madsen, D.; Thomsen, C. L.; Thogersen, J.; Keiding, S. R. Temperature Dependent Relaxation and Recombination Dynamics of the Hydrated Electron. *J. Chem. Phys*. **2000**, *113*, 1126–1134.

30. Elles, C. G.; Jailaubekov, A. E.; Crowell, R. A.; Bradforth, S. E. Excitation-Energy Dependence of the Mechanism for Two-Photon Ionization of Liquid H_2O and D_2O from 8.3 to 12.4 eV. *J. Chem. Phys*. **2006**, *125*, 044515.

31. Hale, G. M.; Querry, M. R. Optical Constants of Water in the 200-nm to 200-μm Wavelength Range. *Appl. Opt*. **1973**, *12*, 555–563.

32. Crowell, R. A.; Lian, R.; Shkrob, I. A.; Qian, J.; Oulianov, D. A.; Pommeret, S. Light-Induced Temperature Jump Causes Power-Dependent Ultrafast Kinetics of Electrons Generated in Multiphoton Ionization of Liquid Water. *J. Phys. Chem. A* **2004**, *108*, 9105–9114.

33. Posthumus, J. H. The Dynamics of Small Molecules in Intense Laser Fields. *Rep. Prog. Phys*. **2004**, *67*, 623–665.

34. Thomsen, C. L.; Madsen, D.; Keiding, S. R.; Thøgersen, J.; Christiansen, O. Two-Photon Dissociation and Ionization of Liquid Water Studied by Femtosecond Transient Absorption Spectroscopy. *J. Chem. Phys*. **1999**, *110*, 3453–3462.

35. Liu, H. T.; Müller, J. P.; Beutler, M.; Ghotbi, M.; Noack, F.; Radloff, W.; Zhavoronkov, N.; Schulz, C. P.; Hertel, I. V. Ultrafast Photo-Excitation Dynamics in Isolated, Neutral Water Clusters. *J. Chem. Phys*. **2011**, *134*, 094305.

36. Trushin, S. A.; Schmid, W. E.; Fuß, W. A Time Constant of 1.8 fs in the Dissociation of Water Excited at 162 nm. *Chem. Phys. Lett*. **2009**, *468*, 9–13.

37. Helm, H.; Bjerre, N.; Dyer, M. J.; Huestis, D. L.; Saeed, M. Images of Photoelectrons Formed in Intense Laser Fields. *Phys. Rev. Lett*. **1993**, *70*, 3221–3224.

38. Kumarappan, V.; Holmegaard, L.; Martiny, C.; Madsen, C. B.; Kjeldsen, T. K.; Viftrup, S. S.; Madsen, L. B.; Stapelfeldt, H. Multiphoton Electron Angular Distributions from Laser-Aligned CS_2 Molecules. *Phys. Rev. Lett*. **2008**, *100*, 093006.

39. Ashihara, S.; Huse, N.; Espagne, A.; Nibbering, E. T. J.; Elsaesser, T. Ultrafast Structural Dynamics of Water Induced by Dissipation of Vibrational Energy. *J. Phys. Chem. A* **2007**, *111*, 743–746.

40. Ingrosso, F.; Rey, R.; Elsaesser, T.; Hynes, J. T. Ultrafast Energy Transfer from the Intramolecular Bending Vibration to Librations in Liquid Water. *J. Phys. Chem. A* **2009**, *113*, 6657–6665.

41. Walrafen, G. E. Raman spectral studies of water structure. *J. Chem. Phys*. **1964**, *40*, 3249–3256.

42. Savikhin, S.; Buck, D. R.; Struve, W. S. Oscillating Anisotropies in Bacteriochlorophyll Protein: Evidence for Quantum Beating Between Exciton Levels. *Chem. Phys*. **1997**, *223*, 303–312.

43. Goulielmakis, E.; Loh; Z.-H.; Wirth, A.; Santra, R.; Rohringer, N.; Yakovlev, V. S.; Zherebtsov, S.; Pfeifer, T.; Azzeer, A. M.; Kling, M. F.; et al. Real-Time Observation of Valence Electron Motion. *Nature* **2010**, *466*, 739–743.

44. Wirth, A.; Hassan, M. T.; Grguraš, I.; Gagnon, J.; Moulet, A.; Luu, T. T.; Pabst, S.; Santra, R.; Alahmed, Z. A.; Azzeer, A. M.; et al. Synthesized Light Transients. *Science* **2011**, *334*, 195–200.

45. Laasonen, K.; Sprik, M.; Parrinello, M.; Car, R. "Ab Initio" Liquid Water. *J. Chem. Phys*. **1993**, *99*, 9080–9089.

46. Prendergast, D.; Grossman, J. C.; Galli, G. The Electronic Structure of Liquid Water within Density-Functional Theory. *J. Chem. Phys*. **2005**, *123*, 014501.

47. Periyasamy, G.; Levine, R. D.; Remacle, F. Electronic Wave Packet Motion in Water Dimer Cation: A Many Electron Description. *Chem. Phys*. **2009**, *366*, 129–138.

48. Baltuška, A.; Emde, M. F.; Pshenichnikov, M. S.; Wiersma, D. A. Early-Time Dynamics of the Photoexcited Hydrated Electron. *J. Phys. Chem. A* **1999**, *103*, 10065–10082.

49. Mukamel, S. *J. Phys. Chem. A* **2013**, DOI: 10.1021/jp408700m.

50. Fecko, C. J.; Eaves, J. D.; Tokmakoff, A. Isotropic and Anisotropic Raman Scattering from Molecular Liquids Measured by Spatially Masked Optical Kerr Effect Spectroscopy. *J. Chem. Phys*. **2002**, *117*, 1139–1154.

51. Heisler, I. A.; Meech, S. R. Low-Frequency Modes of Aqueous Alkali Halide Solutions: Glimpsing the Hydrogen Bonding Vibration. *Science* **2010**, *327*, 857–860.

52. Tauber, M. J.; Mathies, R. A. Resonance Raman Spectra and Vibronic Analysis of the Aqueous Solvated Electron. *Chem. Phys. Lett*. **2002**, *354*, 518–526.

53. Schwartz, B. J.; Rossky, P. J. Pump-Probe Spectroscopy of the Hydrated Electron: A Quantum Molecular Dynamics Simulation. *J. Chem. Phys*. **1994**, *101*, 6902–6916.

54. Yang, C.-Y.; Wong, K. F.; Skaf, M. S.; Rossky, P. J. Instantaneous Normal Mode Analysis of Hydrated Electron Solvation Dynamics. *J. Chem. Phys*. **2001**, *114*, 3598–3611.

55. Triolo, R.; Narten, A. H. Diffraction Pattern and Structure of Aqueous Hydrochloric Acid Solutions at 20^{o}C. *J. Chem. Phys*. **1975**, *63*, 3624–3631.

56. Wang, Q.; Schoenlein, R. W.; Peteanu, L. A.; Mathies, R. A.; Shank, C. V. Vibrational Coherent Photochemistry in the Femtosecond Primary Event of Vision. *Science* **1994**, *266*, 422–424.

57. Zhu, L.; Sage, J. T.; Champion, P. M. Observation of Coherent Reaction Dynamics in Heme-Proteins. *Science* **1994**, *266*, 629–632.

58. Marx, D. Proton Transfer 200 Years after von Grotthuss: Insights from Ab Initio Simulations. *Chem. Phys. Chem*. **2006**, *7*, 1848–1870.

59. Marsalek, O.; Frigato, T.; VandeVondele, J.; Bradforth, S. E.; Schmidt, B.; Schütte, C.; Jungwirth, P. Hydrogen Forms in Water by Proton Transfer to a Distorted Electron. *J. Phys. Chem. B* **2010**, *114*, 915–920.

60. Thürmer, S.; Ončák, M.; Ottoson, N.; Seidel, R.; Hergenhahn, U.; Bradforth, S. E.; Slavičíek, P.; Winter, B. On the Nature and Origin of Dication, Charge-Separated Species Formed in Liquid Water on X-Ray Irradiation. *Nat. Chem*. **2013**, *5*, 590–596.

61. Williams, E. J. Nature of the High Energy Particles of Penetrating Radiation and Status of Ionization and Radiation Formulae. *Phys. Rev*. **1934**, *45*, 729–730.

62. Moshammer, R.; Schmitt, W.; Ullrich, J.; Kollmus, H.; Cassimi, A.; Dörner, R.; Jagutzki, O.; Mann, R.; Olson, R. E.; Prinz, H. T.; et al. Ionization of Helium in the Attosecond Equivalent Light Pulse of 1 GeV/Nucleon U^{92+} Projectiles. *Phys. Rev. Lett*. **1997**, *79*, 3621–3624.